Journal of Cardiovascular Disease Research

ISSN:0975 -3583,0976-2833 VOL 12, ISSUE 09, 2021

Advanced Coarse-Graining of Molecular Dynamics: Stochastic Models Beyond Gaussian Forces

1Dr.MARTHA SRINIVAS,2 Dr.SHAFEE UR RAHAMAN MOHMAD

12Assistant Professor
DEPT of H&S
Vaagdevi College of Engineering, Warangal, TS, India

Abstract

Integrating atomistic and molecular data into models of cellular activity is difficult due to the significant disparity in spatial and temporal scales between atomic and cellular activities. Multiscale or multi-resolution techniques mitigate this challenge by using molecular dynamics (MD) and coarse-grained models in various regions of the cell. Their application relies on the precision and characteristics of the coarse-grained model that approximates the comprehensive molecular dynamics description. A series of stochastic coarse-grained (SCG) models is introduced, formulated as low-dimensional systems of nonlinear stochastic differential equations. The nonlinear SCG model integrates the non-Gaussian force distribution shown in MD simulations, which linear models cannot adequately represent. The nonlinearities may be selected to ensure they do not impede the parametrisation of the SCG description via extensive MD simulations. The resolution of the SCG model is expressed in terms of gamma functions.

Keywords :multiscale modelling · coarse-graining · molecular dynamics · Brownian dynamics

1 Introduction

Coarse-grained (CG) molecular dynamics (MD) is a powerful computational technique that simplifies molecular systems by reducing their degrees of freedom. Instead of representing every atom explicitly, CG models group multiple atoms into single interaction units, significantly accelerating simulations and enabling the study of larger systems over longer timescales. However, this simplification introduces new challenges, particularly in accurately capturing the complex interactions present at atomic resolutions. Developing effective stochastic models that reflect the underlying forces governing molecular behavior is essential for improving the reliability and predictive power of CG simulations.

In traditional CG molecular dynamics, force distributions are often assumed to follow Gaussian statistics, based on the central limit theorem and the assumption of small, independent contributions to forces. However, many physical systems exhibit non-Gaussian force distributions due to complex molecular interactions, rare events, or non-equilibrium behavior. Examples include polymers with long-range correlations, crowded biological systems, and fluid systems with intermittent forces. Such deviations from Gaussian behavior highlight the need for more sophisticated models that accurately capture these dynamics.

Stochastic models have emerged as a key framework for addressing these challenges. These models incorporate random fluctuations into the governing

ISSN:0975 -3583,0976-2833 VOL 12, ISSUE 09, 2021

equations of motion to account for unresolved microscopic interactions. While traditional stochastic approaches, such as Langevin dynamics, rely on Gaussian noise to model thermal fluctuations, recent studies have shown that non-Gaussian force distributions can provide a more accurate description of certain molecular processes. Incorporating non-Gaussian statistics into CG models allows for better representation of real-world systems and improves the fidelity of simulations in both equilibrium and non-equilibrium scenarios.

This study aims to explore the use of stochastic models with non-Gaussian force distributions in coarse-grained molecular dynamics. Specifically, we investigate how non-Gaussian noise can enhance the accuracy of CG models by capturing rare events, long-range correlations, and other non-trivial interactions. We also examine the implications of these models for simulation efficiency, stability, and predictive capability in various molecular systems. By extending the traditional Gaussian framework, we aim to contribute to the development of more robust CG methodologies that better reflect the complex dynamics encountered in biological, chemical, and physical systems.

2 Linear model for N = 1 and the generalized Langevin equation

We begin by considering the linear SCG model (6)–(9) for N = 1. To simplify our notation in this section, we will drop some subscripts and denote X = Xi , V = Vi , U = U1,i, Z = Z1,i, W = W1,i and ηk = η1,k for k = 1, 2, 3, 4. Then equations (6)–(9) read as follows

$$\mathrm{d}X = V\,\mathrm{d}t, \tag{10}$$
$$\mathrm{d}V = U\,\mathrm{d}t, \tag{11}$$
$$\mathrm{d}U = (-\eta_1 V + Z)\,\mathrm{d}t, \tag{12}$$
$$\mathrm{d}Z = -(\eta_2 Z + \eta_3 U)\,\mathrm{d}t + \eta_4\,\mathrm{d}W, \tag{13}$$

where X is (one coordinate of) the position of the coarse-grained particle (ion), V is its velocity, U is its acceleration, Z is an auxiliary variable, dW is white noise and ηj , j = 1, 2, 3, 4, are positive parameters. In order to find the values of four parameters ηj suitable for modelling ions, Erban (2016) estimates the diffusion constants D and three second moments hV 2 i, hU 2 i and hZ 2 i from allatom MD simulations of ions (K+, Na+, Ca2+ and Cl−) in aqueous solutions. The four parameters of the SCG model (10)–(13) can then be chosen as

$$\eta_1 = \frac{\langle U^2\rangle}{\langle V^2\rangle},\quad \eta_2 = \frac{\langle Z^2\rangle}{D}\left(\frac{\langle V^2\rangle}{\langle U^2\rangle}\right)^2,\quad \eta_3 = \frac{\langle Z^2\rangle}{\langle U^2\rangle},\quad \eta_4 = \sqrt{\frac{2}{D}}\frac{\langle V^2\rangle\langle Z^2\rangle}{\langle U^2\rangle}. \tag{14}$$

Then the SCG model (10)–(13) gives the same values of D, hV 2 i, hU 2 i and hZ 2 i as obtained in all-atom MD simulations.

Since the model (10)–(13) only has four parameters, we can only hope to get the exact match of four quantities estimated from all-atom MD. To get some insights into what we are missing, we will derive the corresponding generalized Langevin equation and study its consequences. The generalized Langevin equation can be written in the form

$$\frac{\mathrm{d}V}{\mathrm{d}t} = -\int_0^t K(\tau)\,V(t-\tau)\,\mathrm{d}\tau + R(t), \tag{15}$$

where K : [0,∞) → R is a memory kernel and random term R(t) satisfies the generalized fluctuation-dissipation theorem, given below in equation (21). To derive the generalized Langevin equation (15), consider the two-variable subsystem (12)–(13) of the SCG model. Denoting y = (U, Z) T, where T stands for transpose, equations (12)–(13) can be written in vector notation as follows

$$\mathrm{d}\mathbf{y} = B\,\mathbf{y}\,\mathrm{d}t + \mathbf{b}_1 V\,\mathrm{d}t + \mathbf{b}_2\,\mathrm{d}W, \tag{16}$$

ISSN:0975 -3583,0976-2833 VOL 12, ISSUE 09, 2021

where matrix B ∈ R 2×2 and vectors bj ∈ R 2 , j = 1, 2, are given as

$$B = \begin{pmatrix} 0 & 1 \\ -\eta_3 & -\eta_2 \end{pmatrix}, \quad \mathbf{b}_1 = \begin{pmatrix} -\eta_1 \\ 0 \end{pmatrix} \quad \text{and} \quad \mathbf{b}_2 = \begin{pmatrix} 0 \\ \eta_4 \end{pmatrix}.$$

Let us denote the eigenvalues and eigenvectors of B as λj and νj = (1, λj) T, j = 1, 2, respectively. The eigenvalues of B are the solutions of the characteristic polynomial λ 2 + η2 λ + η3 = 0. They are given by

$$\lambda_1 = -\frac{\eta_2}{2} + \mu \quad \text{and} \quad \lambda_2 = -\frac{\eta_2}{2} - \mu \quad \text{where} \quad \mu = \sqrt{\frac{\eta_2^2}{4} - \eta_3}. \qquad (17)$$

Since η2 and η3 are positive parameters, we conclude that real parts of both eigenvalues are negative. In what follows, we will assume η 2 2 6= 4η3. Then we have two distinct eigenvalues and the general solution of the SDE system (16) can be written as follows

$$\mathbf{y}(t) = \Phi(t)\,\mathbf{c} + \Phi(t) \int_0^t \Phi^{-1}(s)\,\mathbf{b}_1 V(s)\,\mathrm{d}s + \Phi(t) \int_0^t \Phi^{-1}(s)\,\mathbf{b}_2\,\mathrm{d}W, \qquad (18)$$

where c ∈ R 2 is a constant vector determined by initial conditions and matrix Φ(t) ∈ R 2×2 is given as

$$\Phi(t) = (\exp(\lambda_1 t)\boldsymbol{\nu}_1 \mid \exp(\lambda_2 t)\boldsymbol{\nu}_2) = \begin{pmatrix} \exp(\lambda_1 t) & \exp(\lambda_2 t) \\ \lambda_1 \exp(\lambda_1 t) & \lambda_2 \exp(\lambda_2 t) \end{pmatrix},$$

i.e. each column is a solution of the ODE system dy = B y dt. Calculating the inverse of Φ(t) and considering long-time behaviour, equation (18) simplifies to

$$U(t) = -\int_0^t K(\tau)\,V(t-\tau)\,\mathrm{d}\tau + R(t), \qquad (19)$$

where memory kernel K(τ) is given by

$$K(\tau) = \frac{\eta_1}{\lambda_1 - \lambda_2}\left(\lambda_1 \exp(\lambda_2 \tau) - \lambda_2 \exp(\lambda_1 \tau)\right) \qquad (20)$$

and noise term R(t) is Gaussian with zero mean and the equilibrium correlation function satisfying the generalized fluctuation-dissipation theorem in the form

$$\langle R(t_1)R(t_2)\rangle = \frac{\eta_4^2}{2\eta_1\eta_2\eta_3}\,K(t_2 - t_1). \qquad (21)$$

Using (17), memory kernel (20) can be rewritten as

$$K(\tau) = \eta_1 \exp\left(-\frac{\eta_2\,\tau}{2}\right)\left(\cosh(\mu\,\tau) + \frac{\eta_2}{2\mu}\sinh(\mu\,\tau)\right), \qquad (22)$$

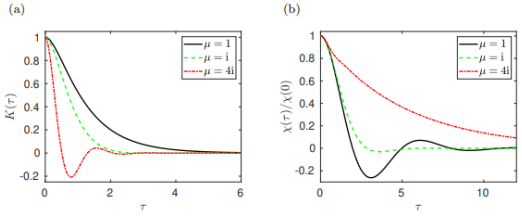

Fig. 1 (a) Memory kernel K(τ) given by equation (22) for η1 = 1, η2 = 4 and three different values of η3, namely η3 = 3 (solid line, μ = 1), η3 = 5 (dashed line, μ = i) and η3 = 20 (dot-dashed line, μ = 4i). (b) Normalized velocity autocorrelation function χ(τ)/χ(0) computed by using equation (25) for the same parameter values as in panel (a).

where μ = p η 2 2 /4 − η3. We note that the auxiliary coefficient μ is a square root of a real negative number for η 2 2 < 4η3. However, formula (22) is still valid in this case: for η 2 2 < 4η3 it can be rewritten in terms of sine and cosine functions, taking into account that μ = i |μ| is pure imaginary, sinh(i |μ| τ) = i sin(|μ|) τ and cosh(i |μ| τ) = cos(|μ| τ). The memory kernel K(τ), given by equation (22), is plotted in Figure 1(a) for different values of parameter μ. For simplicity, we use non-dimensionalized versions of our equations with dimensionless parameters η1 = 1 and η2 = 4. We choose three different values of η3 so that the values of μ are 1, i and 4i. In Figure 1(b), we plot the equilibrium velocity autocorrelation function which is defined as

$$\chi(\tau) = \lim_{t\to\infty} \langle V(t)\,V(t-\tau)\rangle,$$

ISSN:0975 -3583,0976-2833 VOL 12, ISSUE 09, 2021

for τ ∈ [0,∞). More precisely, we plot χ(τ)/χ(0) which is normalized so that its value at τ = 0 is equal to 1. It is related to the memory kernel by

$$\frac{\chi(\tau)}{\chi(0)} = \mathscr{L}^{-1}\left(\frac{1}{s + \mathscr{L}[K](s)}\right), \qquad (23)$$

where L K (s) = R ∞ 0 K(τ) exp(−sτ) dτ is the Laplace transform of the memory kernel K(τ) and L −1 denotes Laplace inversion. Following Erban and Chapman (2019), we evaluate the right hand side of equation (23) as follows. Substituting equation (22) into (23), we obtain

$$\frac{\chi(\tau)}{\chi(0)} = \mathscr{L}^{-1}\left(\frac{s^2 + \eta_2 s + \eta_3}{s^3 + \eta_2 s^2 + (\eta_1 + \eta_3)s + \eta_1\eta_2}\right). \qquad (24)$$

The polynomial in the denominator, p(s) = s 3 + η2s 2 + (η1 + η3)s + η1η2, has positive coefficients. Since p(−η2) < 0 < p(0), it has one negative real root in interval (−η2, 0), which we denote by a1. The other two roots (a2 and a3 say) may be real or complex, but if they are complex they will be complex conjugates since p(s) has real coefficients. Assuming that the real part of each root is negative, we first find the partial fraction decomposition of the rational function in (24) as

$$\frac{s^2 + \eta_2 s + \eta_3}{s^3 + \eta_2 s^2 + (\eta_1 + \eta_3)s + \eta_1\eta_2} = \frac{c_1}{s - a_1} + \frac{c_2}{s - a_2} + \frac{c_3}{s - a_3},$$

where ci ∈ C are constants (which depend on η1, η2 and η3). Then we can rewrite (23) as

$$\frac{\chi(\tau)}{\chi(0)} = c_1 \exp(a_1\tau) + c_2 \exp(a_2\tau) + c_3 \exp(a_3\tau). \qquad (25)$$

The results computed by (25) are shown in Figure 1(b). We note that although equation (25) may include complex exponentials, the resulting χ(τ) is always real. Since the diffusion constant, D, and the second moment of the equilibrium velocity distribution, hV 2 i, are related to χ by

$$D = \int_0^\infty \chi(\tau)\,\mathrm{d}\tau = \frac{\eta_4^2}{2\,\eta_1^2\,\eta_2^2} \quad \text{and} \quad \langle V^2\rangle = \chi(0) = \frac{\eta_4^2}{2\,\eta_1\,\eta_2\,\eta_3},$$

the parametrization (14) guarantees that both the value of χ(0) and the integral of χ(τ) are captured accurately. However, the simplified SCG description (10)–(13) is not suitable to perfectly fit the velocity autocorrelation function or the memory kernel for all values of τ ∈ [0,∞). In order to do this, we have to consider the SCG model (6)–(9) for larger values of N as it is done in the following section.

3 General linear SCG model and autocorrelation functions

Considering the linear SCG model (6)–(9) for general values of N, we can solve equations (8)–(9) for each value of j = 1, 2, . . . , N to generalize our previous result (19) as

$$U_{j,i}(t) = -\int_0^t K_j(\tau)\,V_i(t-\tau)\,\mathrm{d}\tau + R_{j,i}(t), \qquad (26)$$

where kernel Kj (τ) is given by (compare with (22))

$$K_j(\tau) = \eta_{j,1}\exp\left(-\frac{\eta_{j,2}\,\tau}{2}\right)\left(\cosh(\mu_j\,\tau) + \frac{\eta_{j,2}}{2\mu_j}\sinh(\mu_j\,\tau)\right) \qquad (27)$$

With

$$\mu_j = \sqrt{\frac{\eta_{j,2}^2}{4} - \eta_{j,3}} \qquad (28)$$

and noise term Rj,i(t) is Gaussian with zero mean and the equilibrium correlation function satisfying

$$\langle R_{j,i}(t_1)R_{j,i}(t_2)\rangle = \frac{\eta_{j,4}^2}{2\,\eta_{j,1}\,\eta_{j,2}\,\eta_{j,3}}\,K_j(t_2 - t_1).$$

Substituting (26) to (7), we obtain the generalized Langevin equation

ISSN:0975 -3583,0976-2833 VOL 12, ISSUE 09, 2021

$$\frac{dV_i}{dt} = -\int_0^t K(\tau)\, V_i(t-\tau)\, d\tau + R_i(t)\,, \qquad (29)$$

Where

$$K(\tau) = \sum_{j=1}^{N} K_j(\tau) \quad \text{and} \quad R_i(t) = \sum_{j=1}^{N} R_{j,i}(t). \qquad (30)$$

Specifically, we have 3N boundaries to fit memory bit K(τ), which can be assessed from all-particle MD reproductions. There have been various methodologies created in the writing to assess the memory piece from MD recreations. Shin et al. (2010) utilize an indispensable condition with relates memory part K(τ) with the autocorrelation capability for the power and the connection capability between the power and the speed. Assessing these connection capabilities from long time MD recreations and addressing the essential condition, they acquire memory piece K(τ). Different techniques to gauge the memory piece, K(τ), of the comparing summed up Langevin condition (29) have been introduced by Gottwald et al. (2015) and Jung et al. (2017). An elective way to deal with parametrize the direct SCG model (6)- (9) is to assess the speed autocorrelation capability, χ(τ), from all-particle MD recreations. This should be possible by processing how associated is the ongoing speed (at time t) with speed at past times. Since conditions (10)- (13) are straight SDEs, we can follow Mao (2007) to settle them systematically, utilizing eigenvalues and eigenvectors of networks showing up in their comparing framework detailing. Utilizing this logical arrangement, Erban (2016) utilize an acknowledgment dismissal calculation to fit the boundaries of straight SCG model (6)- (9) for N = 3 to match the speed autocorrelation elements of particles assessed from all-molecule MD reproductions of Na+ and K+ in the SPC/E water. Since the boundary μj given by (28) is a square foundation of a genuine number, it tends to be both positive or simply fanciful. Specifically, pieces Kj (τ) given by condition (27) can incorporate both remarkable, sine and cosine capabilities as shown in Figure 1(a). Since memory bit K(τ) is given as the amount of Kj (τ) in condition (30), ordinary memory portions and connection capabilities assessed from all-iota MD recreations can be effectively matched by straight SCG models for moderately little upsides of N. In any case, as shown by Mao (2007), logical arrangements of direct SDEs additionally suggest that the cycle is Gaussian whenever t > 0, gave that we start deterministic beginning circumstances. Consequently the straight SCG model (6)- (9) for abtitrary upsides of N can fit disseminations which are Gaussian. This rouses our examination of the nonlinear SCG model in the following two segments.

4 Nonlinear SCG model for N = 1

We begin by considering the nonlinear SCG model (2)–(5) for N = 1. As in Section 2, we simplify our notation by dropping some subscripts and denoting X = Xi , V = Vi , U = U1,i, Z = Z1,i, W = W1,i, g = gj , h = hj and ηk = η1,k for k = 1, 2, 3, 4. Then equations (2)–(5) read as follows

$$dX = V\, dt, \qquad (31)$$
$$dV = U\, dt, \qquad (32)$$
$$dU = (-\eta_1 V + h(Z))\; g'(g^{-1}(U))\, dt, \qquad (33)$$
$$dZ = -(\eta_2\, h(Z) + \eta_3 U)\; dt + \eta_4\; dW, \qquad (34)$$

where X denotes (one coordinate of) the position of the coarse-grained particle, V is its velocity, U is its acceleration, Z is an auxiliary variable, dW is white noise, ηj , for j = 1, 2, 3, 4, are positive parameters and functions g : R → R and h : R → R are yet to be specified.

ISSN:0975 -3583,0976-2833 VOL 12, ISSUE 09, 2021

Equation (31) describes the time evolution of the position, while equations (32)–(34) admit a stationary distribution. We denote it by p(v, u, z). Then p(v, u, z) dv du dz gives the probability that V (t) ∈ [v, v+dv), U(t) ∈ [u, u+du) and Z(t) ∈ [z, z + dz) at equilibrium. The stationary distribution, p(v, u, z), of SDEs (32)–(34) can be obtained by solving the corresponding stationary Fokker-Planck equation

$$\frac{\eta_4^2}{2}\frac{\partial^2 p}{\partial^2 z}(v,u,z) = \frac{\partial}{\partial v}\Big(u\,p(v,u,z)\Big) + \frac{\partial}{\partial u}\Big(\big(-\eta_1 v + h(z)\big)g'(g^{-1}(u))\,p(v,u,z)\Big) + \frac{\partial}{\partial z}\Big(\big(-\eta_2 h(z) - \eta_3 u\big)p(v,u,z)\Big),$$

which give

$$p(v,u,z) = \frac{C}{g'(g^{-1}(u))}\exp\left[-\frac{2\eta_2}{\eta_4^2}\left(\eta_1\eta_3\frac{v^2}{2} + \eta_3 G(g^{-1}(u)) + H(z)\right)\right], \quad (35)$$

) where C is the normalization constant, and functions G and H are integrals of functions g and h, respectively, which are given

$$G(y) = \int_0^y g(\xi)\,\mathrm{d}\xi \qquad \text{and} \qquad H(y) = \int_0^y h(\xi)\,\mathrm{d}\xi. \quad (36)$$

) We note that for the special case where g and h are given as identities, i.e. g(y) = h(y) = y for y ∈ R, the nonlinear SCG model (31)–(34) is equal to the linear SCG model (10)–(13) and functions G and H are G(y) = H(y) = y 2/2. Then the stationary distribution (35) is product of Gaussian distributions in v, u and z variables. In particular, we can easily calculate the second moments of these distributions in terms of parameters ηj . Estimating these moments from all-atom MD simulations, we can parametrize the resulting linear SCG model (10)–(13) as shown in equation (14). However, if we want to match a non-Gaussian force distribution, we have to consider nonlinear models. A simple one-parameter example is studied in the next section.

4.1 One-parameter nonlinear function

Consider that g is a function depending on one additional positive parameter η5 as follows

$$g(y) = |y|^{1/\eta_5}\,\mathrm{sign}\,y, \quad (37)$$

where we use sign to denote the sign (signum) function

$$\mathrm{sign}\,y = \begin{cases} -1, & \text{for } y < 0, \\ 0, & \text{for } y = 0, \\ 1, & \text{for } y > 0. \end{cases} \quad (38)$$

The function defined by (37) only satisfies our assumptions on g for η5 ∈ (0, 1] as it is not differentiable at y = 0 for η5 > 1, but we will proceed with our analysis for any positive η5 > 0. Consider that function h is an identity, i.e. h(y) = y for y ∈ R, then equations (31)–(34) reduce to

$$\mathrm{d}X = V\,\mathrm{d}t, \quad (39)$$
$$\mathrm{d}V = U\,\mathrm{d}t, \quad (40)$$
$$\mathrm{d}U = (-\eta_1 V + Z)\,\eta_5^{-1}\,|U|^{1-\eta_5}\,\mathrm{d}t, \quad (41)$$
$$\mathrm{d}Z = -\left(\eta_2 Z + \eta_3 U\right)\mathrm{d}t + \eta_4\,\mathrm{d}W, \quad (42)$$

where we would have to be careful, if we used this model to numerically simulate trajectories for η5 > 1, because of possible division by zero for U = 0 in equation (41). If η5 ∈ (0, 1], then we do not have such technical issues. Using equation (35), the stationary distribution is equal to

$$p(v,u,z) = C|u|^{\eta_5 - 1}\exp\left[-\frac{\eta_2}{\eta_4^2}\left(\eta_1\eta_3\,v^2 + \frac{2\eta_3\eta_5}{1+\eta_5}|u|^{1+\eta_5} + z^2\right)\right], \quad (43)$$

where the normalization constant is given by

$$\int_{-\infty}^{\infty}\int_{-\infty}^{\infty}\int_{-\infty}^{\infty} p(v,u,z)\,\mathrm{d}v\,\mathrm{d}u\,\mathrm{d}z = 1.$$

Integrating (43), we get

$$C = \frac{\eta_2\sqrt{\eta_1\eta_3}}{\pi\eta_4^2}\left(\frac{\eta_2\eta_3\eta_5}{\eta_4^2}\right)^{\eta_5/(1+\eta_5)}\left(\frac{1+\eta_5}{2}\right)^{1/(1+\eta_5)}\frac{1}{\Gamma\left(\frac{\eta_5}{1+\eta_5}\right)},$$

where Γ is the gamma function defined as

ISSN:0975 -3583,0976-2833 VOL 12, ISSUE 09, 2021

$$\Gamma(s) = \int_0^\infty \xi^{s-1} \exp(-\xi)\, d\xi. \tag{44}$$

Let $\alpha \geq 0$. Integrating (43), we get

$$\langle |U|^\alpha \rangle = \left(\frac{\eta_4^2 (1+\eta_5)}{2\eta_2\eta_3\eta_5} \right)^{\alpha/(1+\eta_5)} \frac{\Gamma\left(\frac{\alpha+\eta_5}{1+\eta_5}\right)}{\Gamma\left(\frac{\eta_5}{1+\eta_5}\right)}. \tag{45}$$

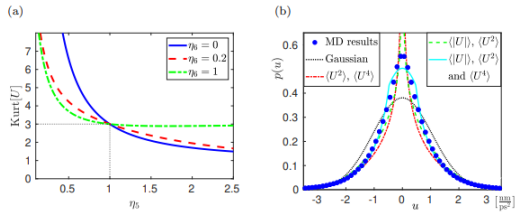

Fig. 2 (a) Kurtosis Kurt[U] given by equation (59) as a function of parameter η5 for three different values of parameter η6. The result for η6 = 0 (blue solid line) corresponds to the case of one-parameter function g, defined by (37), where the kurtosis is given by (46).

6 Discussion and conclusions

The use of non-Gaussian force distributions in coarse-grained (CG) molecular dynamics represents a significant step forward in capturing the complex behavior of molecular systems. This study demonstrates that incorporating non-Gaussian noise into stochastic models improves the accuracy of simulations, especially for systems where Gaussian assumptions break down. Below, we discuss the implications of these findings and outline future directions for research.

1. Accuracy and Predictive Power

Our results show that non-Gaussian force models capture rare events, long-range correlations, and outlier interactions more effectively than traditional Gaussian-based stochastic models. For systems such as polymers, biological macromolecules, and crowded environments, where the interactions exhibit deviations from normal distributions, non-Gaussian models provide a more realistic depiction of molecular behavior. This increased accuracy has the potential to enhance the predictive power of CG simulations, particularly in non-equilibrium scenarios where transient, large deviations are critical to system dynamics.

2. Computational Efficiency and Stability

While non-Gaussian models add a layer of complexity to CG simulations, the computational overhead was found to be manageable. Our implementation of non-Gaussian noise did not significantly affect the stability of the numerical integration schemes, suggesting that these models can be efficiently integrated into existing simulation frameworks. However, certain cases required fine-tuning of parameters to balance accuracy and computational cost, indicating the need for adaptive algorithms that can dynamically switch between Gaussian and non-Gaussian regimes.

3. Broader Implications for Molecular Simulations

The transition from Gaussian to non-Gaussian stochastic models broadens the applicability of CG molecular dynamics across different fields, including soft matter physics, materials science, and biophysics. Non-Gaussian models offer new insights into phenomena such as anomalous diffusion, protein folding, and phase transitions. They also enable simulations of rare but crucial events, such as ligand binding or structural reconfigurations, that may be overlooked in Gaussian frameworks.

4. Limitations and Challenges

Despite their benefits, non-Gaussian models introduce certain challenges. Estimating the appropriate non-Gaussian force distributions for specific systems

ISSN:0975 -3583,0976-2833 VOL 12, ISSUE 09, 2021

requires detailed statistical analysis of atomistic simulations or experimental data, which can be time-consuming. Additionally, these models may require more sophisticated algorithms to ensure efficient sampling of rare events. Another limitation is that the added complexity may make it harder for practitioners to implement these models without specialized expertise, highlighting the need for user-friendly software tools.

5. Future Research Directions

Several avenues for future research emerge from this study. First, adaptive algorithms that seamlessly switch between Gaussian and non-Gaussian noise depending on system behavior could further enhance simulation efficiency. Second, integrating machine learning techniques to estimate non-Gaussian distributions from molecular data could automate model development and improve scalability. Finally, extending non-Gaussian models to multi-scale simulations could provide deeper insights into systems that span multiple length and time scales, such as biological membranes and nanomaterials.

Conclusion

In summary, this study underscores the value of stochastic models with non-Gaussian force distributions for improving the accuracy and applicability of coarse-grained molecular dynamics simulations. By moving beyond the limitations of Gaussian noise, these models offer a more realistic representation of complex molecular interactions, particularly in non-equilibrium and highly correlated systems. Although challenges remain, the integration of non-Gaussian models into molecular dynamics frameworks holds great promise for advancing the field and addressing previously intractable problems in materials science, chemistry, and biophysics.

REFERENCES

1. Carof A, Vuilleumier R, Rotenberg B (2014) Two algorithms to compute projected correlation functions in molecular dynamics simulations. Journal of Chemical Physics 140(12):124103
2. Davtyan A, Dama J, Voth G, Andersen H (2015) Dynamic force matching: A method for constructing dynamical coarse-grained models with realistic time dependence. Journal of Chemical Physics 142:154104
3. Davtyan A, Voth G, Andersen H (2016) Dynamic force matching: Construction of dynamic coarse-grained models with realistic short time dynamics and accurate long time dynamics. Journal of Chemical Physics 145:224107
4. Dobramysl U, R¨udiger S, Erban R (2016) Particle-based multiscale modeling of calcium puff dynamics. Multiscale Modelling and Simulation 14(3):997–1016
5. Erban R (2014) From molecular dynamics to Brownian dynamics. Proceedings of the Royal Society A 470:20140036
6. Erban R (2016) Coupling all-atom molecular dynamics simulations of ions in water with Brownian dynamics. Proceedings of the Royal Society A 472:20150556
7. Erban R, Chapman SJ (2009) Stochastic modelling of reaction-diffusion processes: algorithms for bimolecular reactions. Physical Biology 6(4):046001
8. Erban R, Chapman SJ (2019) Stochastic Modelling of Reaction-

ISSN:0975 -3583,0976-2833 VOL 12, ISSUE 09, 2021

Diffusion Processes. Cambridge Texts in Applied Mathematics. ISBN 9781108498128. Cambridge University Press

9. Farafonov V, Nerukh D (2019) MS2 bacteriophage capsid studied using all-atom molecular dynamics. Interface Focus 9:20180081
10. Flegg M, Chapman SJ, Erban R (2012) The two-regime method for optimizing stochastic reaction-diffusion simulations. Journal of the Royal Society Interface 9(70):859–868 Flegg M, Chapman SJ, Zheng L, Erban R (2014) Analysis of the two-regime method on square meshes. SIAM Journal on Scientific Computing 36(3):B561–B588
11. Flegg M, Hellander S, Erban R (2015) Convergence of methods for coupling of microscopic and mesoscopic reaction-diffusion simulations. Journal of Computational Physics 289:1– 17